Algebraic Reconstruction for Magnetic Resonance Imaging Under B_0 Inhomogeneity

Yasser M. Kadah and Xiaoping Hu* *Member, IEEE*

***Abstract*—In magnetic resonance imaging, spatial localization is usually achieved using Fourier encoding which is realized by applying a magnetic field gradient along the dimension of interest to create a linear correspondence between the resonance frequency and spatial location following the Larmor equation. In the presence of B_0 inhomogeneities along this dimension, the linear mapping does not hold and spatial distortions arise in the acquired images. In this paper, the problem of image reconstruction under an inhomogeneous field is formulated as an inverse problem of a linear Fredholm equation of the first kind. The operators in these problems are estimated using field mapping and the k-space trajectory of the imaging sequence. Since such inverse problems are known to be ill-posed in general, robust solvers, singular value decomposition and conjugate gradient method, are employed to obtain corrected images that are optimal in the Frobenius norm sense. Based on this formulation, the choice of the imaging sequence for well-conditioned matrix operators is discussed, and it is shown that nonlinear k-space trajectories provide better results. The reconstruction technique is applied to sequences where the distortion is more severe along one of the image dimensions and the two-dimensional reconstruction problem becomes equivalent to a set of independent one-dimensional problems. Experimental results demonstrate the performance and stability of the algebraic reconstruction methods.**

***Index Terms*— B_0 inhomogeneity, distortion correction, fast imaging, image reconstruction, MRI.**

I. Introduction

In Fourier imaging, spatial localization is achieved by applying linear magnetic field gradients to impose a precise linear mapping between spatial locations and their resonance frequencies as dictated by the Larmor equation. Imperfections of the static magnetic field, the magnetic field gradients, or significant changes in the susceptibility within the imaged field-of-view (FOV) can lead to image distortions and artifacts [1], [2]. This problem is present to some degree with all magnetic resonance imaging (MRI) techniques, but its severity widely varies amongst different imaging sequences as well as between different dimensions for the same sequence. For example, in spin-echo (SE) images, the distortion is present along the readout (and to a lesser extent along slice selection directions) and is moderate. Severe distortions are usually encountered with echo planar imaging (EPI) along the phase encoding direction. Possible image distortions include pixel shift and/or deformation (i.e., compression or expansion), which is accompanied by intensity modulations [1], [3]. Pixel shift arises when a difference exists between the field at a given pixel and that of the static magnetic field. On the other hand, pixel deformations arise from a field gradient across individual pixels, which also leads to intensity modulations as a result of the nonunity Jacobian of the distorted space-frequency mapping. While rectifying the distortions is possible in some cases, it may not be achieved in cases when the field inhomogeneity maps different pixels in the original into an identical position in the image. In these cases, it is generally not possible to obtain a correct reconstruction of this image without additional information.

Various methods have been suggested and implemented to overcome the problem of inhomogeneity-induced image distortions. These techniques can be generally classified into two main categories according to the way the inhomogeneity inverse operator is designed. The first category includes the methods based on field mapping. Field maps can be used to correct shifts in the spatial domain by computing the expected pixel displacement and unwarping the image [4]–[7], or to modify the k-space data in a pixel-specific manner as with the conjugate phase method [8], [9]. Other techniques use field maps to derive analytical models for the distorted space-frequency mapping in different simplified forms that allow for fast correction [10]. Finally, there was an attempt to solve the inhomogeneity problem algebraically by inverting a very large approximate matrix operator to derive a vector composed of the whole image [11].

The second category of correction techniques are those that do not require field mapping. The most important of such methods is the one that uses two images acquired with gradients of reversed polarity [12]. Since the inhomogeneity effect does not change between the two images, the direction of the resultant distortions is opposite between the two. Hence, by comparing the two, it is possible to derive a distortion-free image.

While existing correction techniques provide satisfactory results in many situations, it should be noted that methods in both categories correspond to approximate inverses of the inhomogeneity distortion operator. Consequently, the correction results are not optimal. Therefore, a reconstruction method

Manuscript received August 18, 1997; revised April 10, 1998. This work was supported by the National Institutes of Health (NIH) under Grants RO1MH55346 and RR08079. The Associate Editor responsible for coordinating the review of this paper and recommending its publication was Y. Censor. *Asterisk indicates corresponding author.*

Y. M. Kadah is with the Department of Radiology, Center for Magnetic Resonance Research, and Biomedical Engineering Program, University of Minnesota, Minneapolis, MN 55455 USA.

*X. Hu is with the Department of Radiology, Center for Magnetic Resonance Research, and Biomedical Engineering Program, University of Minnesota, 385 East River Road, Minneapolis, MN 55455 USA (e-mail: hu@sparky.drad.umn.edu).

Publisher Item Identifier S 0278-0062(98)06442-8.

that is based on solving for the inverse of the inhomogeneity operator such that the norm of the error is minimum can be advantageous.

In this paper, we describe an algebraic model and an optimal solution to the problem of B_0 inhomogeneity distortion correction. The continuous case is first considered and shown to be a Fredholm integral equation of the first kind. A discretization strategy is proposed to translate the continuous problem into a linear system of equations that can be solved numerically to obtain the least-squares solution. Several numerical methods of different characteristics are described to compute this solution in an accurate and stable fashion under linear constraints. The dependence of the algebraic model on the imaging sequence is also considered, and it is shown that in general nonlinear k-space trajectories provide better results than linear ones. Finally, the performance of the approach is demonstrated by experimental data using single-shot and segmented with centric reordering blipped-EPI imaging sequences, where the problem is essentially one-dimensional (1-D) with the distortion mainly occurring along the phase encoding direction.

II. Theory

A. Continuous Problem Formulation

Consider the case of Fourier imaging of a 1-D object of spatial intensity $f(x)$ in the presence of field inhomogeneity represented by $\Delta B(x)$. The resultant continuous k-space of this object $F_d(k)$ takes the form

$$F_d(k) = \int_{-\infty}^{\infty} f(x) \cdot e^{j\gamma \Delta B(x) \cdot t(k)} \exp\{-j2\pi kx\} dx. \quad (1)$$

Here, γ is the gyro magnetic ratio and $t(k)$ is a time function that depends on the k-space trajectory of the imaging sequence. This equation represents a linear Fredholm integral equation of the first kind with kernel, $K_I(x,k) = e^{j\gamma \Delta B(x) \cdot t(k)} \exp\{-j2\pi kx\}$ [15]. That is, the k-space data can be expressed as the outcome of applying a linear operator $\mathcal{T}$ to the original or *true* spatial intensity such that

$$F_d = \mathcal{T}(f). \quad (2)$$

Throughout this paper, $\mathcal{T}$ will be referred to as the *transformation* operator since it performs the mapping between the original object and the k-space taking into account the inhomogeneity effects. An equivalent formulation can be generated by premultiplying (2) with $\mathcal{T}^*$, the conjugate operator. In this case, the operator equation is expressed in terms of the so-called *Grammian* operator defined as $\mathcal{G} = (\mathcal{T}^* \cdot \mathcal{T})$. Another interesting operator equation arises when (2) is premultiplied by the inverse Fourier transform operator, $\mathcal{F}^*$. The operator in this equation will be referred to as the *deformation* operator $\mathcal{D} = (\mathcal{F}^* \cdot \mathcal{T})$ because the original object function f is mapped directly to the resultant distorted spatial distribution f_d. Since these three operator equations are equivalent, the choice of the one to use depends on the desirable features each offers as applied to the specific solution method at hand. Examples of such features include the transformation operator being Vandermonde in some cases, the Grammian operator being Hermitian, and the deformation operator being sparse.

In general, an operator $\mathcal{A}$ can be fully described by a mapping rule from the Hilbert space of its domain to that of its range. The mapping rule is defined by the available information about the data-acquisition procedure. The reconstruction problem becomes one of finding an inverse operator $\mathcal{A}^\dagger$ such that

$$\left(\mathcal{A}^\dagger \cdot \mathcal{A}\right) = \mathcal{I} \quad (3)$$

where $\mathcal{I}$ is the *identity operator*. Then, the solution to the original problem of finding f is given by

$$\mathcal{A}^\dagger(F_d) = \left(\mathcal{A}^\dagger \cdot \mathcal{A}\right)(f) = \mathcal{I}(f) = f. \quad (4)$$

In general, the mapping rule that defines the operator may not be one-to-one. In this case, the operator is *singular*, and it is not possible to construct the inverse operator. In some other cases, the operator maps different points in its domain to different yet very close points in its range. If these points are too close, slight contamination with additive noise can render them indistinguishable, making it difficult to compute the inverse operator. In such cases, the operator is *ill posed* [13] and it is only possible to seek a regularized inverse operator to obtain an approximate solution.

When an operator over the Hilbert space is ill posed or singular, its domain can be divided into the minimum-norm space spanned by all minimum-norm solutions to the inverse problem, and the null space of the operator. Since the null and minimum-norm subspaces are orthogonal and together they are complete, least-squares solutions correspond to the summation of two components: the minimum-norm solution and any available data, and any function in the null subspace. In MRI, the inhomogeneity operator may have blinds pots defined by the null space in its domain, and the components of the input spatial distribution that lie within these spots cannot be recovered. In this case, several forms of optimal solutions can be considered. The first one is the minimum-norm or minimal least-squares solution which corresponds to the special case when the null space component is chosen to be zero. Given the definition of the null space and some general constraints on the solution based on *a priori* information about the imaged object, alternative solutions can be formulated by adding functions in the null space to the minimum norm solution such that these constraints are satisfied [21].

Observing that the operator in this problem is a linear operator, it is possible to obtain a solution based on full-rank operator composition achieved by reducing the size of the null space with over sampling. Oversampling can be achieved by using multiple scans with different k-space trajectories or taking more samples than dictated by the sampling requirements of conventional Fourier imaging (see, [12]). In the absence of magnetic field inhomogeneities, oversampling would be considered redundant. Nevertheless, when magnetic field inhomogeneities exist, oversampling is needed to improve the conditioning of the operator equation and reduce the null space.

B. Discretization

For practical implementation, it is necessary to discretize the original problem before attempting to obtain the solution. The discretization can be achieved in a variety of ways that approximate the integral with a finite sum. In general, the discretized problem takes the form

$$\sum_{n=1}^{N} w_n K_I(k, x_n) \cdot f(x_n) = F_d(k) \tag{5}$$

where w_n are weights that are functions of the discretization rule. Notice that in practice it is only possible to collect limited extent, discrete samples in the k-space. Therefore, *collocation* is invoked to convert the above equation to the desired finite-dimensional problem [15]. That is, to force the continuous equation to hold at specified discrete points such that

$$\sum_{n=1}^{N} w_n K_I(k_m, x_n) \cdot f(x_n) = F(k_m), \quad m = 1, 2, \cdots, M. \tag{6}$$

In this case, the original integral equation is approximated by an $M \times N$ linear system, $\mathbf{A}\vec{f} = \vec{F_d}$, where $\mathbf{A}$ is an $M \times N$ matrix with entries $[w_n K_I(k_m, x_n)]$, $\vec{f}$ is an $N \times 1$ vector with entries $[f(x_n)]$, and $\vec{F_d}$ is an $M \times 1$ vector with entries $[F_d(k_m)]$. That is, the discretization of the operator $\mathcal{T}$ is the matrix $\mathbf{A}$, and the operator $\mathcal{T}^*$ is represented by the matrix $\mathbf{A}^*$, the conjugate transpose of the matrix $\mathbf{A}$. The most common approach to evaluate the weights w_n is the *midpoint rule*, where a numerical integration rule (e.g., Simpson's rule) is applied to the continuous integral, yielding a sum with equal and constant weights (ignoring edge effects). Therefore, up to a constant multiplier, the weights for the midpoint rule are given as

$$w_n^{\text{midpoint}} = 1, \qquad n = 1, 2, \cdots, N. \tag{7}$$

It should be noted that the discretization of an ill-posed integral equation of the first kind yields an *ill-conditioned* linear system. In general, the higher the resolution of this discretization, the closer the finite-dimensional problem to the ill-posed continuous problem and, consequently, the more ill conditioned the algebraic problem becomes [15]. Given that the size of common MRI inhomogeneity correction problems is equal to the matrix size along the direction of interest (e.g., the phase-encoding direction for EPI), which is usually large (around 128), the ill conditioning of the algebraic problem is expected to be severe. Therefore, the numerical solution methods to be used to solve this problem must be able to maintain robust performance under these conditions in order to obtain a stable inverse to this system.

C. Inhomogeneity Problem in EPI: From Two-Dimensional (2-D) to 1-D

In EPI, the data acquisition time is negligible along one of dimensions and $t(k_x, k_y)$ can be considered as a function of one component, i.e., $t(k_x, k_y) \approx t(k_y)$. In this case, the 2-D k-space data take the form

$$F_d(k_x, k_y) = \int\int_{-\infty}^{\infty} f(x, y) \cdot e^{j\gamma \Delta B(x,y) \cdot t(k_y)} \cdot \exp[-j2\pi(k_x x + k_y y)]\, dx\, dy \tag{8}$$

where $f(\cdot, \cdot)$ is the true signal within the imaged slice, $F_d(\cdot, \cdot)$ is the collected k-space data, $\Delta B(\cdot, \cdot)$ is the corresponding inhomogeneity field map, and $t(\cdot)$ is a function of the k-space time trajectory. Performing a 1-D inverse Fourier transform operation with respect to k_x on both sides of the above formula, we obtain

$$\hat{F}_d(x_o, k_y) = \int_{-\infty}^{\infty} f(x_o, y) \cdot e^{j\gamma \Delta B(x_o,y) \cdot t(k_y)} \cdot \exp[-j2\pi k_y y]\, dy \tag{9}$$

where $\hat{F}_d(\cdot, \cdot)$ is the inverse Fourier transform of $F_d(\cdot, \cdot)$with respect to the first dimension. As can be seen, this form is equivalent to the 1-D problem where the given data are the k-space representation of the object, the inhomogeneity field map, and the k-space time trajectory, while the unknown is the spatial distribution along a line in the image defined by $x = x_o$. Hence, by solving a set of 1-D problems that sufficiently sample the image structure in the x-dimension, the 2-D problem is solved.

It should be noted that the above discussion is general for EPI since no particular form for $t(k)$ in (9) was assumed. Examples of possible forms of this function include $t(k) = \text{constant} \times k$ for single-shot blipped-EPI (i.e., single echo acquisition in which the transition between different rows is achieved using small gradient pulses or *blips*), and $t(k) = \text{constant} \times |k|$ for segmented blipped-EPI with centric reordering (i.e., acquisition is performed using two echoes or *segments*, one for positive k_y and one for negative k_y values of the k-space area of interest, in a similar fashion to blipped-EPI starting from the center of the k-space).

D. Example of a Matrix Operator

As an example, the case of a single-shot blipped-EPI imaging sequence is examined in this section. The midpoint discretization method is used and the corresponding linear system is derived. In this particular case, the problem can be formulated such that the discrete transformation operator $\mathcal{T}$ is a Vandermonde matrix of the form [16]

$$\mathbf{V} = \begin{bmatrix} 1 & 1 & \cdots & 1 \\ \lambda_o & \lambda_1 & \cdots & \lambda_N \\ \lambda_0^2 & \lambda_1^2 & \cdots & \lambda_N^2 \\ \vdots & \vdots & & \vdots \\ \lambda_0^N & \lambda_1^N & \cdots & \lambda_N^N \end{bmatrix}. \tag{10}$$

This matrix is completely defined by only one row in the form: $[\lambda_0 \lambda_1 \cdots \lambda_N]$, which is usually called the Vandermonde coefficient vector. This can be of great advantage for reducing the storage space when the matrix is large or when the number of systems to be solved is large. For our problem, the elements of the Vandermonde coefficient vector corresponding to the

transformation operator take the form

$$\lambda_n = e^{j\gamma\Delta B(x_o, y_n)\cdot\Delta k} \cdot \exp[-j2\pi y_n \cdot \Delta k] \qquad (11)$$

where Δk is the step size in the k-space. The matrix corresponding to the Grammian operator of this Vandermonde system is a member of the class of Hilbert matrices [20]. Also, the columns of the deformation operator are related to the Vandermonde transformation operator through a Fourier transform. Given that each column of the Vandermonde matrix corresponds to samples of a complex exponential, it is expected that each column of the deformation matrix will contain only a few nonzero elements. In fact, if the sampling scheme happens to be appropriate for the particular frequency of a given column, its corresponding deformation matrix column will contain only one element. In other words, the number of nonzero elements depends on the sampling scheme and the field inhomogeneity, but is generally much smaller than the size of the matrix. Hence, the deformation matrix is *sparse* [14]. Moreover, the elements of this matrix are generally expected to be largely centered around the main diagonal. Therefore, it can be considered as a constant bandwidth sparse matrix with a bandwidth determined by the maximum deviation from the diagonal.

In addition to the possible computational and storage advantages of the deformation matrix formulation, it also provides an explicit visualization of the inhomogeneity induced distortion. When there is no inhomogeneity at a particular location, the matrix column corresponding to this location is equal to the corresponding column of an identity matrix. Conversely, when there is an inhomogeneous field at a certain location, two possible scenarios can be encountered corresponding to a shifted version of an identity matrix column, and a blur extending over a number of locations around the nonzero element. Given the deformation matrix, it is possible to identify the presence of overlap among distortions from neighboring pixels by inspecting its rows. In particular, when a given row contains more than one nonzero element, more than one pixel in the original image contribute to a single pixel in the distorted image. When there are such overlaps, shift-based correction methods fail. Therefore, it may be advantageous to use this matrix to analyze the inhomogeneity effects before resorting to a particular correction method. An example of this matrix is shown in Fig. 1.

It should be noted that a similar analysis can also be performed for the general case of nonlinear $t(k)$ such as segmented blipped-EPI. In this case, the transformation operator is not a Vandermonde matrix and the deformation matrix is still sparse but expected to have a wider bandwidth because of the extra blur associated with the point-spread functions of such sequences.

E. Imaging Sequence Dependence

It is interesting to examine the dependence of the condition number of the imaging operators on the imaging sequence. As can be seen from the above example, the operator matrix is a function of $t(k)$, which is defined by the k-space trajectory of the imaging sequence. Therefore, the condition number of the operators depends on the form of $t(k)$.

Fig. 1. Illustration of an actual deformation matrix obtained with single-shot blipped EPI. The mapping looks distorted from the ideal form of a diagonal line.

In general, ill-posed operators are those which are close to singular operators. Therefore, a good criterion for assessing the well posedness of an operator is to check for possible singularities under small perturbations in its parameters. When singularities exist, it is expected that the operator will generally be ill posed in practice. On the other hand, if there are no singularities, the operator is expected to maintain its well posedness.

In order to apply this criterion here, an inhomogeneity operator is applied to two points at different locations in the FOV (without loss of generality). Deriving the singularity condition is equivalent to determining the conditions under which the outcome of applying the operator in both cases is the same. If such conditions exist, the operator contains singularities and practical matrix operators are expected to be ill conditioned, and vice versa. The signals from two points located at x_1 and x_2 with magnetic field inhomogeneities $\Delta B(x_1)$ and $\Delta B(x_2)$ are given by

$$r_1(k) = e^{-j2\pi k x_1} \cdot e^{j\gamma\Delta B(x_1)t(k)} \qquad (12)$$

and

$$r_2(k) = e^{-j2\pi k x_2} \cdot e^{j\gamma\Delta B(x_2)t(k)}. \qquad (13)$$

Usually these signals are observed for a finite interval, say $[-1/2, 1/2)$. In order to assess the independence of these signals, the inner product of the two signals over the observation period is evaluated as

$$\langle r_1, r_2\rangle = \int_{-1/2}^{1/2} e^{-j2\pi k(x_2 - x_1)} \cdot e^{j\gamma(\Delta B(x_2) - \Delta B(x_1))t(k)} dk. \qquad (14)$$

Let $\Delta n = x_2 - x_1$ and $\Delta b = \gamma(\Delta B(x_2) - \Delta B(x_1))$, and define the distortion function $d(k; \Delta b) = e^{j\Delta b t(k)}$. Assuming the periodicity of the k-space and invoking Parseval's identity of the Fourier transform, the inner product can be written in

the form

$$\langle r_1, r_2\rangle = \sum_n \delta(n-\Delta n)D(n;\ \Delta b) = D(\Delta n;\ \Delta b). \quad (15)$$

Here $D(n;\ \Delta b)$ is the inverse discrete-time Fourier transform of $d(k;\ \Delta b)$, where n is the spatial distance in pixels, and $\delta(.)$ is the Kronecker delta function. Hence, the result of the inner product depends mainly on the value of the Fourier transform of the distortion function. When singularities exist, this inner product becomes equal to the square of the norm of either signal, indicating that the two signals are identical. In other words, when the contributions from two different pixels are identical, it is impossible to separate the individual contributions of these pixels.

Now consider the two main functional forms of $t(k)$, namely, linear and nonlinear functions. In the first, such as with single-shot blipped-EPI, $t(k) = \alpha k$, and the outcome of the inner product takes the form

$$\langle r_1, r_2\rangle_{\text{linear}} = \delta(\Delta n - \alpha\Delta b). \quad (16)$$

As a result, the operator in this case will be singular at all points with locations and inhomogeneities satisfying $\Delta n = \alpha\Delta b$. Hence, the matrix operators in this case are ill conditioned. This can be intuitively seen because $r_1(k) = r_2(k)$ everywhere when $x_2 - x_1 = \alpha\Delta b$ for $t(k) = \alpha k$. This happens (but may not if the inhomogeneity is not too large) for linear $t(k)$ since Fourier encoding is linear in k. This is not the case when $t(k)$ is nonlinear regardless of the magnitude of the inhomogeneity. For example, consider the case of a segmented blipped-EPI with centric reordering, where $t(k) = \alpha|k|$. In this case, the inner product takes the form

$$\begin{aligned}\langle r_1, r_2\rangle_{\text{nonlinear}} &= \tfrac{1}{2}\big(\delta(n-\Delta n+\alpha\Delta b)\\ &\quad + \delta(n-\Delta n-\alpha\Delta b)\big) + \frac{1}{2\pi j}\\ &\quad \cdot\left(\frac{1}{n-\Delta n+\alpha\Delta b} - \frac{1}{n-\Delta n-\alpha\Delta b}\right).\end{aligned} \quad (17)$$

Two main conclusions can be drawn from (17). First, the inner product becomes a single δ-function only in the trivial case when $\Delta n = \alpha\Delta b = 0$. Second, the maximum values of this form occur at $n = \pm\alpha\Delta b$, and is equal to approximately half the result in the trivial case. As a result, the matrix operators for this sequence are expected to be better-conditioned than for sequences having linear trajectories. Therefore, from a theoretical point of view, it is always advantageous to use nonlinear k-space trajectories when inhomogeneity distortions exist and are to be corrected for in the reconstruction.

III. Numerical Solution Methods

A. SVD Solver

As discussed above, eigen-decomposition or singular value decomposition (SVD) can be used to identify the null space of a given linear system and to obtain the least squares solution. Given the superior numerical properties of the SVD, it is usually the method of choice for this computation. Using SVD, any N-dimensional matrix operator, $\mathbf{A}$, can be expressed in an orthogonal representation of the form

$$\mathbf{A} = \mathbf{U}\mathbf{\Sigma}\mathbf{V}^T = \sum_{n=1}^{N} \sigma_n \vec{u}_n \vec{v}_n^{\,T} \quad (18)$$

where σ_n is the nth singular value and $\vec{u}_n$ and $\vec{v}_n$ are members of the ortho-normal sets of vectors in the columns of $\mathbf{U}$ and the rows of $\mathbf{V}$, spanning the space of N-dimensional (N-D) vectors. In the case when the system is well conditioned, the inverse of the matrix operator $\mathbf{A}$ is given as

$$\mathbf{A}^{\dagger} = \sum_{n=1}^{N} \frac{1}{\sigma_n} \vec{u}_n \vec{v}_n^{\,T}. \quad (19)$$

On the other hand, when the system is ill conditioned, small singular values may be of the same order as the usual numerical noise encountered in this computation. In this case, to avoid artifacts from the basis vectors corresponding to those very small singular values, the method of truncated SVD (TSVD) can be used to provide stable solutions that are optimal in the least-square sense. In this method, the singular values are thresholded and only those above the threshold are included in the summation of (19). With appropriate selections of the truncation level, TSVD is a regularization method. As with any regularization method for ill-posed problems, the choice of the truncation threshold is critical. For a fixed amount of noise, the TSVD will begin to diverge if the truncation level is increased beyond a certain level. It should be noted that choosing the truncation level can be shown to be equivalent to imposing a quadratic constraint on the solution.

B. Conjugate Gradient Method (CGM)

Among known robust linear system solvers, the CGM proposed originally by Hestenes and Stiefel [18], [19] is considered one of the most efficient. This method describes a class of iterative techniques having the desirable property of guaranteed convergence in a finite number of iterations. Also, even when the system is ill conditioned, good estimates of the largest and smallest eigenvalues are not needed to determine the algorithm parameters. The basic idea of this method is to eliminate the residual error $\vec{e} = \mathbf{A}\cdot\vec{x}_{sol} - \vec{b}$ in a linear system $\mathbf{A}\vec{x} = \vec{b}$, along mutually $\mathbf{A}$-orthogonal directions spanning the space of the solution [19], [21]. The original formulation of this technique requires the system to be real, square, symmetric, and positive definite for the algorithm to work and provide the unique solution to the system. In this work, a direct modification of the technique is applied to complex Hermitian, positive semidefinite linear systems to compute the minimal least-square solution. That is, it is used to solve the normal equations of the system given the properties of the Grammian matrix defined by $\mathbf{G} = \mathbf{T}^*\cdot\mathbf{T}$.

The conjugate gradient algorithm for solving the normal equation $\mathbf{A}^*\mathbf{A}\vec{\mathbf{x}} = \mathbf{A}^*\vec{\mathbf{b}}$ is described as follows:

1) Set the initial solution $\vec{x}_o$ as the distorted object.
2) Compute the initial residual $\vec{r}_o = \vec{b} - \mathbf{A}\vec{x}_o$.
3) Compute first direction $\vec{p}_o = \mathbf{A}^*\vec{r}_o$.

4) Compute $c_m = ||\mathbf{A}^*\vec{r}_m||_2^2$, $d_m = ||\mathbf{A}\vec{p}_m||_2^2$, and $a_m = c_m/d_m$.
5) Update solution $\vec{x}_{m+1} = \vec{x}_m + a_m \cdot \vec{p}_m$, and update residual $\vec{r}_{m+1} = \vec{r}_m - a_m \cdot \mathbf{A}\vec{p}_m$.
6) Compute $e_m = ||\mathbf{A}^*\vec{r}_{m+1}||_2^2/c_m$, and update direction $\vec{p}_{m+1} = \mathbf{A}^*\vec{r}_{m+1} + e_m \cdot \vec{p}_m$.
7) Increment counter $m = m + 1$, and repeat steps 4) through 6) until one of the following termination conditions is satisfied: $e_m = 0$, c_m is below a given threshold, or the number of iterations reached a predetermined number N.

Two main points about this algorithm are noted. First, the initial solution vector is chosen as the distorted image. Unlike any other initials election, this particular choice uses the available information to ensure that the solution after any number of iterations is better in the least-squares sense than the distorted image. This choice may also reduce the number of iterations needed to reach a given accuracy. Second, the termination condition should ideally be that the norm of the residual $\vec{r}_k$ goes to zero if the system has a full rankor when the parameter c_k goes to zero if the system is rank-deficient. Even though these conditions will eventually be met in a finite number of iterations, a large fraction of the iterations contribute to an insignificant improvement in the solution. In particular, when c_k is extremely small yet nonzero, the correction term is multiplied by a very small value and hence do not amount to a noticeable change in the results. Therefore, in our implementation, the termination condition was set as c_k being smaller than a predetermined threshold.

In theory, the CGM reaches a unique solution or the minimal least square solution in less than N steps, where N is the size of the linear system [18]. Moreover, if the linear system matrix can be expressed as the sum of the identity matrix and another matrix $\mathbf{C}$ of rank r_C, the algorithm converges in no more than $r_C + 1$ steps. Hence, the convergence is fast in general and only a few steps may be needed to reach a solution with reasonable accuracy. The complexity of this method is estimated as $O(N^2)$ flops/iteration/line, which can be significantly lower than that of SVD when a few iterations are used.

C. Solution Constraining

When the linear system matrix is ill conditioned, it is always advantageous to impose certain constraints on the solution based on *a priori* information regarding the physical system being imaged. In general, constraining improves the accuracy of the result and amounts to regularization in most cases. One type of constraints that can be useful for our problem is linear equality constraints, which are often invoked when certain parts of the FOV are known *a priori*. For example, when the FOV is larger than the imaged object, equality constraints can be applied to force the solution at the points outside the object boundaries to be zero.[1] In general, equality constraints can be expressed as $\mathbf{B} \cdot \vec{x} = \vec{d}$, where $\mathbf{B}$ is a $P \times N$ full-rank matrix and $\vec{d}$ is a P-dimensional vector. The exact application of the general form of this equation involves a QR decomposition step, which is rather computationally prohibitive, especially when the solver is chosen to be the CGM [21]. Nevertheless, in practice, it is sufficient to adhere to the constraints only approximately. This allows the constraints to be invoked with only a small added complexity by concatenating the constraint equation to the original linear system with a weighting factor and solving the composite system. In this case, the solution satisfies the constraint more closely as the weighting factor gets larger. It should be noted, however, that numerical stability can be affected rather severely for large values of this weighting factor. A reasonable value for this parameter is of the order of the estimated average singular value of the linear system matrix, usually of the order of ten. When the $\mathbf{B}$ matrix is diagonal, the solution method can be modified to solve only for all pixels that are not assigned values by the constraints. In this case, the solution satisfies the constraints in the exact sense.

[1] It should be noted that in EPI Nyquist ghosts of significant energy are often encountered and c. Application of equality constraints in the ghost regions may force artifactual image energy into the central reconstruction region and degrade image quality

IV. Methods

The reconstruction methods described here were applied to experimental data of phantoms and human volunteers acquired on a 1.5-T Siemens Magnetom Vision MR scanner. The images were acquired using either a single-shot blipped-EPI sequence or a segmented blipped-EPI with centric reordering with a TE of 70 ms and a TR of 200 ms. The FOV was 31 cm $\times$ 31 cm and the matrix size was 128 $\times$128. In our implementation, the field maps are computed from two images acquired using a FLASH sequence with slightly different TE values prior to the actual data acquisition. The resultant field maps are masked based on the image intensity to eliminate erratic field values in regions with very low signal [6]. Subsequently, the field map is smoothed using a spatial domain low-pass filter for noise reduction [4]. These two steps were found to be crucial to the quality of the solution of the resultant linear system. For an $N \times N$ images, the field maps are used to construct N linear systems of equations based on the k-space trajectory of the imaging sequence as discrete versions of (9). The midpoint rule was used to perform this discretization as described in (6) and (7). Each of these linear systems is concatenated with a set of equations corresponding to linear constraints and supplied to either the TSVD solver or the CGM solver to obtain one column in the corrected image. The linear constraints are imposed to force the solution to approach zero in the empty areas in the FOV. The threshold used with the TSVD solver was selected to be unity for our experiment.[2] For the CGM solver, two iterations were used.

V. Experimental Results

In Figs. 2 and 3, the results of the two-iteration CGM on phantom and human data acquired using single-shot blipped-EPI and segmented blipped-EPI with centric reordering imag-

[2] It should be noted that in general the choice of this threshold is a function of the matrix size. However, for the relatively narrow range of matrix sizes used in practical MRI, this choice of unity apply well throughout.

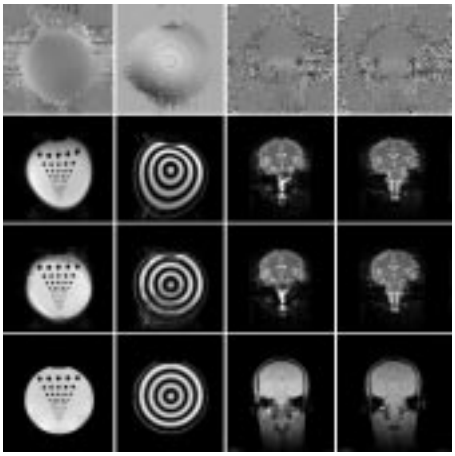

Fig. 2. Correction of single-shot blipped-EPI data with two-iteration conjugate gradient iteration. Images from top to bottom are: field maps, distorted images, corrected images, and FLASH comparison images.

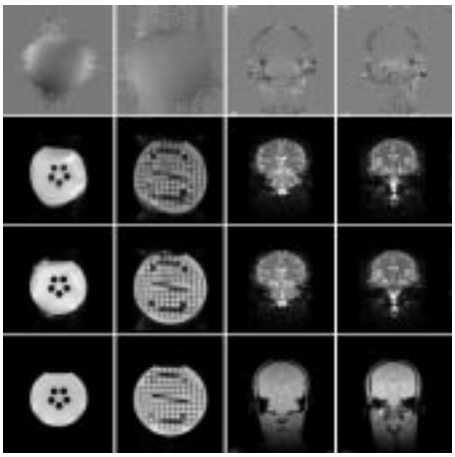

Fig. 3. Correction of data acquired using segmented blipped-EPI with centric reordering imaging sequence with two-iteration conjugate gradient iteration. Images from top to bottom are: field maps, distorted images, corrected images, and FLASH comparison images.

ing sequences are illustrated. By comparison to the FLASH images, it can be seen that the correction improves the geometric accuracy in both phantom and human images with both sequences while maintaining reasonable computational efficiency.

In Figs. 4 and 5, the results of using the TSVD solver to correct images acquired with single-shot blipped-EPI and segmented blipped-EPI with centric reordering are illustrated. In Fig. 4, images obtained with single-shot blipped-EPI and segmented blipped-EPI with centric reordering are shown as examples of linear and nonlinear trajectory sequences. The range of B_0 variation was between -164 and $+167$ Hz. Even though the original image obtained with the latter sequence exhibits more severe distortion artifacts combining geometric shift and blurring, the quality of corrected images from this sequence is superior to that with single-shot blipped-EPI, in agreement with the theoretical prediction. In Fig. 5, the same comparison is applied to human data and a similar conclusion can be drawn. The ranges of B_0 variation in these images were from -94 to $+100$ Hz for the coronal scan.

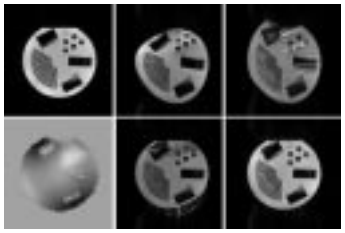

Fig. 4. Comparison of single-shot blipped-EPI and segmented blipped-EPI with centric reordering for phantom data. Images in the left column represent the FLASH comparison image and the field map. In the middle column, the distorted and SVD corrected images with single-shot blipped-EPI, while those in the right column are for segmented blipped-EPI.

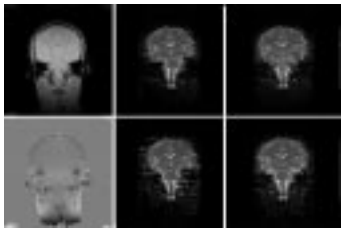

Fig. 5. Comparison of single-shot blipped-EPI and segmented blipped-EPI with centric reordering for human data. Images in the left column represent the FLASH comparison image and the field map. In the middle column, the distorted and SVD corrected images with single-shot blipped-EPI, while those in the right column are for segmented blipped-EPI.

VI. Discussion

In practice, the experimental information is often contaminated with additive noise. As a result, the processes of eigenvalue decomposition and SVD are perturbed by this noise thus producing all nonzero eigenvalue and singular value sets even when the operator is singular. In this case, the theoretical null space is equivalent to the noise subspace that can be detected using one of many likelihood ratio criteria. If a zero-mean white Gaussian noise model is assumed, this detection process amounts to a simple absolute value thresholding of the resultant eigenvalues or singular values as in TSVD.

It is also important to consider the contamination of field maps with noise and its effect on the reconstruction. To assess this problem, a combination of measurements and simulations were performed to arrive at the following observations. After performing a number of independent field mapping measurements for the same slice, the results from all measurements were found to be within only 4 Hz from their average, a good estimate of the true field map. From computer simulations, it was evident that when the field deviations are within 5 Hz, fairly accurate reconstruction is expected. Therefore, the results from the field mapping procedure are generally stable. Smoothing and low-intensity masking of field maps were also found to be of important value in improving the stability of the procedure even further.

When the matrix operator takes the form of a Vandermonde matrix, the first solver that comes to mind is the Vandermonde matrix solver proposed by Bjork and Pereyra [15] which is known for its reduced complexity. However, when the matrix is ill conditioned or rank-deficient as with cases of severe inhomogeneity, this solver cannot be used since regularization disrupts the characteristic form of the matrix required

by the solver. Without regularization, the solution becomes dominated by numerical instabilities that are functions not only of the condition number of the system matrix but also of the machine epsilon (a measure of the numerical accuracy of a machine defined as the smallest number that does not get truncated when added to unity [17]). Therefore, this solver cannot be used for our application because of its lack of robustness.

Two important features should be noted about the SVD solution method. First, it explicitly computes the inverse operator and in doing that, it requires only information about the system matrix $\mathbf{A}$. Given that the matrix operator is usually estimated by field mapping before the actual acquisition of the distorted data, the process of SVD computation can be performed prior to the actual data acquisition, assuming perfect registration between the field map and the subject imaged subsequently. The second important feature of SVD is that it explicitly identifies the null space of the matrix operator. Hence, when different k-space traversal methods are available for data acquisition, they can be compared based on the dimensionality of their corresponding null spaces. In other words, we can make an *a priori* choice of the scanning method that would yield the best solution. For example, if the operator matrix forms for single-shot blipped-EPI and segmented blipped-EPI with centric reordering sequences are examined, it can be shown that the latter is more stable and is therefore expected to maintain full rank under the same conditions that cause the former to be rank-deficient. Moreover, if a full-rank solution is required, it is possible to devise a k-space traversal strategy to provide a full-rank operator equation from several scans. In this case, the tradeoff between the amount of acquired data and the solution accuracy can be directly addressed with this method. Although this solver is flexible, it is associated with a rather high computational complexity [$O(N^3)$ flops/line] that is a determining disadvantage in many situations.

Even though the computational complexity of the SVD solver seems rather prohibitive in general, this might not be the case for applications where repeated images of the same slices are obtained. For example, in functional imaging, a time sequence of as many as hundreds of acquisitions of the same slice is obtained to assess brain activation during the time course of an experiment. In this case, SVD inverse matrix operator can be computed once and used to correct all images in the time series. The resultant complexity will be comparable to that of the conjugate phase method while maintaining the least-squares optimality of the correction.

As suggested by the theory, given a field map, it is possible to compare the performance of different scanning sequences prior to the actual data acquisition by comparing the condition numbers of their system matrices. An interesting observation in this aspect is that only linear trajectory sequences may have rank-deficient system matrices. This is a direct result of their linear phase evolution characteristics, which are similar to those of the Fourier transform matrix columns. With nonlinear scanning sequences such as segmented blipped-EPI or spiral, the phase evolution characteristics are rather distinct from those of Fourier vectors and, hence, their system matrices are of full rank. Therefore, our theoretical result indicates that the use of nonlinear k-space trajectories leads to better reconstructions under B_0 inhomogeneity.

It should be noted that the CGM does not explicitly identify the null space of the system and that the remaining residual after algorithm termination lies in that space. It is therefore not possible to define the null space using CGM. As a result, this method cannot be used to derive a strategy for full-rank system composition from oversampling as with SVD.

An interesting special case of the CGM procedure occurs when only one iteration is used. In this case, the CGM amounts to an approximate correction method similar to the conjugate phase method proposed by Maeda *et al.* [8]. In fact, it can be shown that the conjugate phase method is a special case of the conjugate gradient iterative solver when the initial solution is zero and the number of iterations is exactly one. Hence, several strategies can be employed to take advantage of this observation. First, a generalized multistep conjugate phase method can be directly implemented by using the conjugate gradient iterations. An alternative approach to the conjugate phase method can also be proposed when the initial solution is chosen as the distorted object. The possible advantage of using this method is the guaranteed lower error norm. This is not generally the case with the conjugate phase method.

VII. Conclusions

Stable algebraic reconstruction methods for MRI under severe magnetic field inhomogeneity are described. The present approach is based on estimating the operator that produces the distorted images and computing the least-squares inverse operator that can be applied to derive corrected images. The corrected images are, therefore, optimal in the Frobenius-norm sense. This formalism allows a theoretical comparison of imaging sequences with different trajectories in terms of the stability of the algebraic reconstruction problem, suggesting that nonlinear k-space trajectory sequences such as segmented blipped-EPI with centric reordering provide better results than linear trajectory sequences as single-shot blipped-EPI. Two methods were described to compute the solution. The first is based on TSVD and provides an optimal solution at the cost of high computational complexity. The second method, the CGM, provides a fast approximation to TSVD solution where the accuracy of this approximation is controlled by the choice of the number of iterations. Finally, these reconstruction methods were successfully demonstrated with experimental data in which the distortion was mainly along one of the image dimensions. The clinical potential of these methods remains to be addressed in future studies.

References

[1] F. Farzaneh, S. J. Riederer, and N. J. Pelc, "Analysis of T2 limitations and off-resonance effects on spatial resolution and artifacts in echo-planar imaging," *Magn. Reson. Med.*, vol. 14, pp. 123–139, 1990.

[2] T. Sumanaweera, G. Glover, S. Song, J. Adler, and S. Napel, "Quantifying MRI geometric distortion in tissue," *Magn. Reson. Med.*, vol. 31, pp. 40–47, 1994.

[3] T. S. Sumanaweera, G. H. Glover, T. O. Binford, and J. R. Adler, "MR susceptibility misregistration correction," *IEEE Trans. Med. Imag.*, vol. 12, pp. 251–259, June 1993.

[4] K. Sekihara, M. Kuroda, and H. Kohno, "Image restoration from nonuniform magnetic field influence for direct Fourier NMR imaging," *Phys. Med. Biol.*, vol. 29, no. 1, pp. 15–24, 1984.
[5] K. Sekihara and H. Kohno, "Image restoration from nonuniform static field influence in modified echo-planar imaging," *Med. Phys.*, vol. 14, no. 6, pp. 1087–1089, 1987.
[6] P. Jezzard and R. S. Balaban, "Correction for geometric distortion in echo planar images from Bo field variations," *Magn. Reson. Med.*, vol. 34, pp. 65–73, 1995.
[7] R. M. Weisskoff and T. L. Davis, "Correcting gross distortions on echo planar images," in *Proc. SMRM 11th Annu. Meet.*, Berlin, 1992, p. 4515.
[8] A. Maeda, K. Sano, and T. Yokoyama, "Reconstruction by weighted correlation for MRI with time-varying gradients," *IEEE Trans. Med. Imag.*, vol. 7, pp. 26–31, Mar. 1988.
[9] D. C. Noll, C. H. Meyer, J. M. Pauly, D. G. Nishimura, and A. Macovski, "A homogeneity correction method for magnetic resonance imaging with time-varying gradients," *IEEE Trans. Med. Imag.*, vol. 10, pp. 629–637, Dec. 1991.
[10] P. Irarrazabal, C. H. Meyer, D. G. Nishimura, and A. Macovski, "In homogeneity correction using an estimated linear field map," *Magn. Reson. Med.*, vol. 35, pp. 278–282, 1996.
[11] L.-C. Man, J. M. Pauly, and A. Macovski, "Correcting severe local inhomogeneity blurs by spatially variant deconvolution," in *Proc. SMRM 3rd Annu. Meet.*, Nice, 1995, p. 738.
[12] H. Chang and J. M. Fitzpatrick, "A technique for accurate magnetic resonance imaging in the presence of field inhomogeneity," *IEEE Trans. Med. Imag.*, vol. 11, pp. 319–329, Sept. 1992.
[13] A. Bakushinsky and A. Goncharsky, *Ill-Posed Problems: Theory and Applications.* London, U.K.: Kluwer, 1994.
[14] U. Schendel, *Sparse Matrices.* New York: John Wiley and Sons, 1989.
[15] C. W. Groetsch, *Inverse Problems in the Mathematical Sciences.* Braunschweig, Germany: Vieweg, 1993.
[16] A. Bjorck and V. Pereyra, "Solution of Vandermonde systems of equations," *Math. Computation*, vol. 24, pp. 893–903, 1970.
[17] W. Gautchi, "Optimally conditioned Vandermonde matrices," *Numerische Mathematische*, vol. 24, pp. 1–12, 1975.
[18] M. R. Hestenes and E. Stiefel, "Methods of conjugate gradients for solving linear systems," *J. Res. Nat. Bur. Standards*, vol. 49, pp. 409–436, 1952.
[19] M. R. Hestenes, *Conjugate Direction Methods in Optimization.* Heidelberg, Germany: Springer-Verlag, 1980.
[20] G. Heinig and K. Rost, *Algebraic Methods for Toeplitz-Like Matrices and Operators.* Stuttgart, Germany: Birkhauser Verlag, 1984.
[21] G. Golub and C. F. Van Loan, *Matrix Computations.* Baltimore, MD: Johns Hopkins Univ. Press, 1989.